REVIEW ARTICLE
https://doi.org/10.1038/s43588-021-00140-w

nature computational science

Computational design of quantum defects in two-dimensional materials

Yuan Ping[1]✉ and Tyler J. Smart[2,3]

Missing atoms or atom substitutions (point defects) in crystal lattices in two-dimensional (2D) materials are potential hosts for emerging quantum technologies, such as single-photon emitters and spin quantum bits (qubits). First-principles-guided design of quantum defects in 2D materials is paving the way for rational spin qubit discovery. Here we discuss the frontier of first-principles theory development and the challenges in predicting the critical physical properties of point defects in 2D materials for quantum information technology, in particular for optoelectronic and spin-optotronic properties. Strong many-body interactions at reduced dimensionality require advanced electronic structure methods beyond mean-field theory. The great challenges for developing theoretical methods that are appropriate for strongly correlated defect states, as well as general approaches for predicting spin relaxation and the decoherence time of spin defects, are yet to be addressed.

Point defects such as missing atoms (vacancies) in a crystal lattice play an important role in semiconductor physics and often determine a system's electronic, optical and transport properties. Defect properties have proven to be an essential tuning knob for optimizing the efficiency of solar cells, semiconductor transistors, light-emitting diodes and catalysts. Recently, point defects in extremely thin materials and two-dimensional (2D) materials have attracted wide research interest, mainly due to the presence of intriguing optoelectronic, spin-optotronic and catalytic properties. These emergent properties enable novel applications in energy technologies and, more importantly, quantum information technology—a new generation of information technology based on quantum bits (qubits) as information carriers and processor registers. Two-dimensional materials bring additional benefits compared with traditional bulk materials, allowing, for example, easier integration into smaller solid-state devices because of their atomically thin thickness. Among the many well-known 2D materials, hexagonal boron nitride (hBN)[1–3] and transition metal dichalcogenides (TMD)[4–6] are considered two of the most promising material platforms for hosting point defects that can be used to emit a single quantum of light or photon (single-photon emitters, SPEs) at room temperature[4,5,7] or potentially used as solid-state qubits. These SPEs and qubits are the building blocks for quantum information technology devices. More importantly, the strong magnetic-field-dependent photoluminescence observed in hBN indicates the presence of optically addressable defects with unpaired spins, which are defined as spin defects[8]. These observations make defects (more specifically spin defects) in 2D materials promising for next-generation SPEs and qubits[9,10].

However, major challenges persist and need to be addressed for the further rational design and development of defects in 2D materials as SPEs or qubits (also referred to as 2D quantum defects). These challenges include (1) difficulty in identifying the chemical nature of an experimentally observed SPE signal and (2) for modeling in particular, the scarcity of reliable theory that can accurately predict the critical physical properties for defects in 2D materials. To address the first of these challenges, tremendous efforts have been made to identify the origin of experimentally observed SPEs. Possible candidates include carbon impurities[11–13], boron dangling bonds[14,15] and N anti-sites with vacancies (N substitution of B accompanying a nitrogen vacancy (NV))[16–18] for hBN, chalcogen vacancies for TMDs[6,19,20], as well as dislocations and Stone–Wales impurities for other 2D materials[21,22]. Notably, the negatively charged boron vacancy in hBN has uniquely emerged as an intrinsic triplet ground-state defect that is promising for quantum information science applications[23–25]. Meanwhile, tremendous progress has been made to address the second challenge in relation to theory and computational modeling; this will be the focus of this Review.

We will first discuss the theoretical design criteria for 2D defects and, with these principles in mind, we will consider how recent methodological developments can help in the rational design of 2D defects. To rationally design promising defects in 2D materials for quantum information science applications, several important conditions need to be met: deep defect levels, high spin states, high radiative recombination rates, weak electron–phonon coupling and long spin relaxation (T_1) and coherence (T_2) times[9]. Deep defect levels help increase the fidelity of stored quantum information, which means that the quantum defects must be designed with their energy levels well separated from the band edges to avoid resonance with the bulk band edges[9,10]. High spin states (for example, two parallel unpaired spins) are necessary for the initialization, operation and readout of spin qubits[26]. The radiative recombination rate being greater than the non-radiative rate ensures a high quantum efficiency of the SPEs and high readout efficiency of spin qubits[9]. Weak coupling with the environmental bath (for example, phonons and nuclear spins) provides a long spin lifetime (spin relaxation time T_1 and coherence time T_2) at room temperature, thus maximizing the lifetime of the stored information and minimizing qubit error. By using these criteria to screen all possible candidates in the periodic table, new quantum defects in 2D materials can be proposed from first-principles calculations, that is, only relying on quantum mechanics, without prior input parameters. Promising candidates can be further validated by means of various experimental techniques, including materials synthesis, scanning microscopy for

[1]Department of Chemistry and Biochemistry, University of California, Santa Cruz, CA, USA. [2]Department of Physics, University of California, Santa Cruz, CA, USA. [3]Lawrence Livermore National Laboratory, Livermore, CA, USA. ✉e-mail: yuanping@ucsc.edu

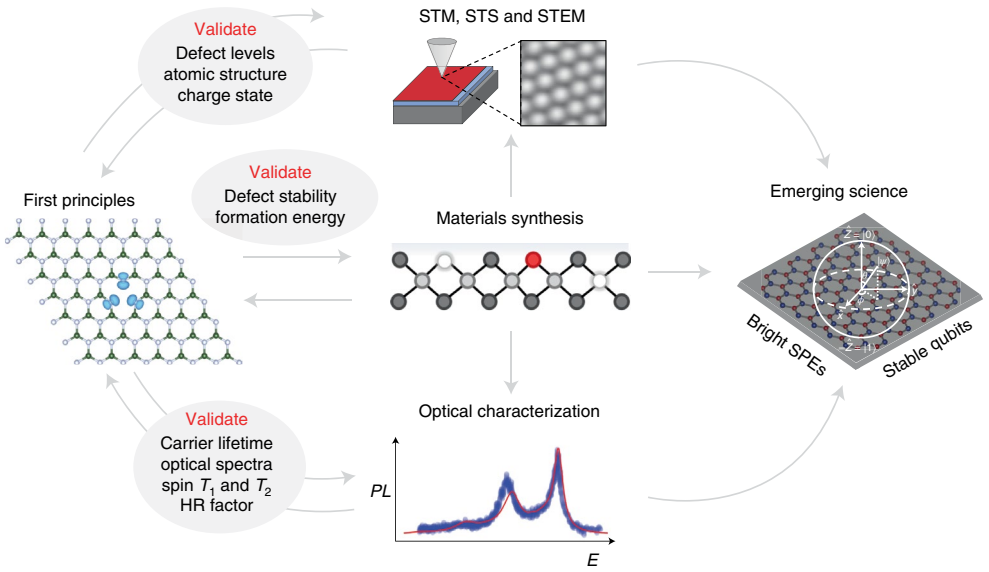

Fig. 1 | A proposed feedback loop between theory and experiments for new spin defect discovery in 2D materials. The first-principles design of spin defects, targeting physical properties to obtain bright SPEs and stable spin qubits for quantum information applications, validated by experiments including surface characterization techniques, materials synthesis and optical characterization. Specifically, calculations of defect levels, charge state and atomic structure can be validated by scanning tunneling microscopy (STM), scanning tunneling spectroscopy (STS) and scanning transmission electron microscopy (STEM) measurements. The defect thermodynamic stability, obtained by computing the defect formation energy, can be confirmed by materials synthesis. Finally, the calculated exciton lifetime, optical spectra (including absorption and photoluminescence spectroscopy, PL), spin relaxation time (T_1), spin coherence time (T_2) and the Huang–Rhys (HR) factor can be validated by optical characterization techniques from experiments.

analyzing the electronic structure and local atomic structure, as well as optical characterization (Fig. 1). The experiment–theory feedback loop is an effective strategy for new spin defect development and spin qubit design.

Compared with 3D systems, there are unique theoretical challenges in accurately predicting critical defect properties in 2D materials, stemming from the highly anisotropic dielectric screening and strong many-body interactions in two dimensions, including electron–hole, exciton–phonon and defect–exciton interactions (Fig. 2), which are beyond the capability of standard density functional theory (DFT) codes at the mean-field theory level. Specifically, the confined dimension leads to weak screening along the out-of-plane direction. This causes problems when using mean-field theory-based methods, such as failure of the electronic structure description, severe periodic image charge interactions for charged defects and inaccurate description of optical signatures from defect–exciton couplings. Accordingly, advanced methods beyond the treatment of electrons at the DFT level, such as many-body perturbation theory with the *GW* approximation (*G* is Green's function and *W* is screened Coulomb interaction) for electronic states and solving the Bethe–Salpeter equation (BSE) for two-particle absorption spectra, are often necessary for the accurate description of such interactions. We will discuss potential ways to address these theoretical challenges in the following.

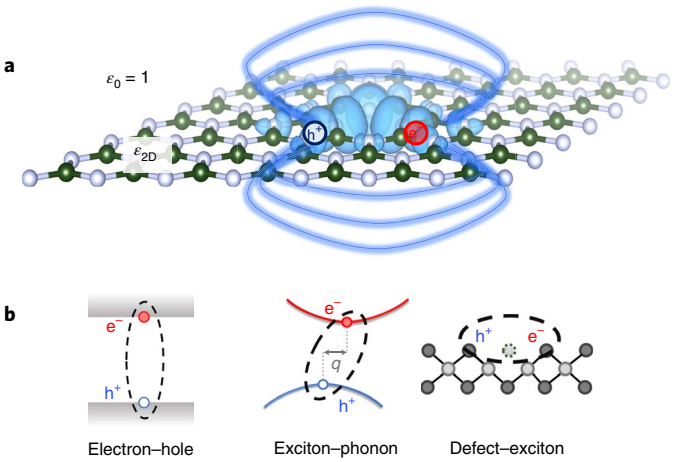

Fig. 2 | Reduced dielectric screening in 2D systems leads to strong many-body interactions, profoundly affecting defect properties. a, The electric field lines (blue) between an electron (e^-) and a hole (h^+), which together compose a bound exciton, are mostly outside the material (monolayer hBN is used as an example, with green spheres denoting B atoms and white spheres N atoms). Outside the material, the dielectric screening is weak, with a dielectric constant (ε_0) equal to 1. **b**, Owing to the weak screening in **a**, the electron–hole, exciton–phonon and defect–exciton interactions are much stronger, which fundamentally determines the physical properties of quantum defects in 2D materials.

Thermodynamics modeling of 2D quantum defects

Defect formation energy and charge transition levels. Defect formation energies (E^f) and charge transition levels (CTLs) are the fundamental properties of defects in solids, with the former representing how easily a defect can form under a specific chemical condition (such as temperature and oxygen partial pressure) and the latter how easily a defect can be ionized to form a charged state. Two-dimensional charged defects are ubiquitous and of essential technical relevance. For example, the experimentally identified B vacancy in hBN is negatively charged and provides an important magnetic-field-dependent optical response for spin qubit applications[23–25].

With periodic boundary conditions, isolated defects are created computationally by placing defects in large cells composed of many crystal unit structures (defect 'supercell' calculation) so as to reduce

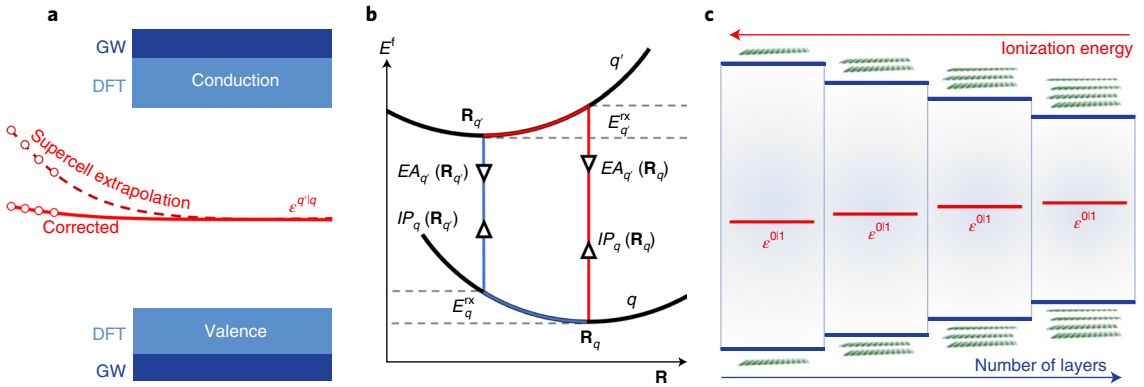

Fig. 3 | Calculation of the CTLs of defects in 2D systems. a, The CTL (denoted $\epsilon^{q'/q}$) in a 2D system, obtained with charge correction (solid line, corrected) or using the supercell extrapolation method to converge the supercell sizes (dashed line, supercell extrapolation). The band edge can be obtained more accurately at the *GW* level or approximately with DFT with semi-local exchange correlation functionals. **b**, The defect formation energy (E^f) as a function of configuration coordinate (**R**) at charge states q and q'. $\mathbf{R}_q$ ($\mathbf{R}_{q'}$) denotes the equilibrium structure at charge state q (q'). The vertical excitation energy between two charge states (vertical red and blue lines) is related to the IP in charge state q at coordinate $\mathbf{R}_q$ ($IP_q(\mathbf{R}_q)$) or $\mathbf{R}_{q'}$ ($IP_q(\mathbf{R}_{q'})$) or alternately is related to the EA in charge state q' at coordinate $\mathbf{R}_q$ ($EA_{q'}(\mathbf{R}_q)$) or $\mathbf{R}_{q'}$ ($EA_{q'}(\mathbf{R}_{q'})$). The relaxation energy at one charge state from a configuration coordinate away from equilibrium to the equilibrium position is denoted by $E^{rx}_{q'}$. The CTL $\epsilon^{q'|q}$ related to the energy difference between the minima at two formation-energy surface curves can be calculated by two pathways (red and blue), which involve computing accurate IP or EA values and a relaxation energy (E^{rx}). **c**, The CTL position ($\epsilon^{0|1}$, with red lines) and band edge of bulk states (blue levels) shift systematically as a function of number of hBN layers, and the ionization energy (energy difference between $\epsilon^{0|1}$ and the conduction band edges) decreases consistently with increasing layer thickness.

the interactions between defects in the central supercell and their periodic images. The corresponding defect formation energy E^f at a particular charge state q and geometry **R** can be expressed as

$$E^f_q(\mathbf{R}_q) = E_{tot}(\mathbf{R}_q) - E_{tot}(\text{host}) - \sum_i n_i\mu_i + q\epsilon_F + \Delta_q \quad (1)$$

where E_{tot} is the total energy of the defect supercell or the pristine host (host), n_i are the differences in the number of atoms for each element between the pristine and defective systems, μ_i are their elemental chemical potentials and ϵ_F is the Fermi level of the pristine host. The interaction between defects in the central supercell and their periodic images decays more slowly with monopole (charged defects) than neutral defects. Such spurious interactions lead to large errors, for example, on the order of several electronvolts[27]. Δ_q is the defect charge correction that corrects for the spurious interactions between periodic charges.

The calculation of Δ_q is critical for reliable supercell convergence of a charged defect at a non-interacting limit. Owing to the weak and highly anisotropic screening in 2D systems, the charge correction Δ_q is more difficult than for their 3D counterparts and needs to recover the proper electrostatic interaction of a charge in an ultrathin 2D plane. Several different strategies have been proposed for 2D defect charge corrections[28–37]. Their underlying principles mainly fall into two categories. One approach is to derive analytical expressions for the electrostatic energies of point charges in a 2D dielectric medium as a function of supercell size, then the correct limit can be obtained by supercell extrapolation based on these expressions[28]. The other approach is to use the model charge electrostatic self-energy difference between isolated (open boundary condition, V_{iso}) and periodic (V_{per}) boundary conditions to approximate the spurious interactions introduced by an extra electron or hole, and then remove the self-energy difference between the two boundary conditions from the defect formation energy[29–34]. Sundararaman and Ping[35] analytically derived an exact expression for the isolated boundary condition for 2D systems using a spectral expansion technique that eliminated supercell extrapolation, where a high-order polynomial fit is specifically needed for 2D systems[31]. Wu et al.[33] defined an anisotropic dielectric profile for ultrathin 2D systems, which can be directly derived from regularized DFT electrostatic potentials and applied to the charged defect formation energy in ultrathin hBN (Fig. 3a). The model charge method in the second category only needs one supercell calculation, which is substantially cheaper than the former extrapolation method, which requires several supercell calculations. However, the model charge distribution is more properly defined when the excess charge is relatively localized.

Recently, self-consistent charged defect correction methods have been proposed for 2D defects, where a self-consistent potential correction is applied in the calculations of total energies, eigenvalues and forces[36,38]. Analogous to the model charge method described in the previous paragraph, V_{iso} and V_{per} are used to determine the corrective potential due to charged defects. The major difference is that the extra charge in the supercell ($\delta\rho$) is determined from the difference between the electronic density of the charged defect system (ρ^{chg}) and the reference (neutral, ρ^{ref}) system on a real-space grid, $\delta\rho(r) = \rho^{chg}(r) - \rho^{ref}$, instead of a model charge such as a point or Gaussian charge as used in previous calculations[29–34]. The corrective potential is then added to the total potential and solved self-consistently. This method prevents the formation of an artificial state in the vacuum (as sometimes arises as a result of the applied counter charge potential), which could not be removed by previous methods. Note that, although the different charge correction schemes result in similar results for charge correction (for example, within 0.1 eV), as benchmarked previously[31,39], they have very different computational costs and applicability.

The thermodynamic CTL. A CTL is defined as the value of the electron chemical potential ($\epsilon^{q'|q}$) at which the stable charge state of the defect changes from q to q'. Accordingly, the ionization energy of a defect can be computed by measuring the distance between the CTL and the band edges in the band diagram. The CTL can be mathematically calculated by imposing that the formation energies of the q and q' states are equal, as given by

$$\epsilon^{q'|q} = E^f_q(\mathbf{R}_q) - E^f_{q'}(\mathbf{R}_{q'}) = \underbrace{E^f_q(\mathbf{R}_q) - E^f_{q'}(\mathbf{R}_q)}_{E_{QP}} + \underbrace{E^f_{q'}(\mathbf{R}_q) - E^f_{q'}(\mathbf{R}_{q'})}_{E^{rx}} \quad (2)$$

where $\mathbf{R}_q$ ($\mathbf{R}_{q'}$) are the ionic coordinates of charge states q (q') and E_q^f is the formation energy of a charged defect at charge state q, as defined in equation (1). The total energy difference at different charge states as inputs for equation (2) involves the electron ionization potential (IP) and electron affinity (EA)[29], which cannot be accurately obtained at the standard DFT level, although the total energy differences between different structures at the same charge state are much more accurate with DFT. Accordingly, $\epsilon^{q'|q}$ can be separated into two parts, as shown in the right side of equation (2) and schematically with a red curve in Fig. 3b, with a vertical excitation energy (E_{QP}) from the q state to the q' state at the equilibrium geometry of charge state q ($\mathbf{R}_q$), plus a geometry relaxation energy (E^{rx}) at the same charge state q'. A second pathway to separate into E_{QP} and E^{rx} is depicted with a blue curve in Fig. 3b; in principle, this provides identical results[37,38]. E^{rx} can be obtained with reasonable accuracy by standard DFT as long as a reliable charge correction Δ_q has been obtained, as discussed already.

To obtain an accurate quasiparticle energy E_{QP} (vertical ionization or EA energy) for defects in 2D materials, accurate electron correlation needs to be taken into account. Considering that point defects often have molecular orbitals such as wavefunctions around defect centers, they contribute negligibly to the dielectric screening of whole systems. Accordingly, the criteria for choosing a methodology are largely determined by how well they describe the corresponding 2D host systems. Note that the anisotropic screening in 2D systems makes conventional DFT methods such as the Heyd–Scuseria–Ernzerhof (HSE) hybrid functional with a fixed Hartree–Fock exchange[40] rather unreliable. For example, with increasing number of layers from monolayer to bulk hBN, the electronic bandgap obtained at the HSE level is rather unchanged, with a variation of within 0.2 eV, which is in sharp contrast to the results with the *GW* level, with a lowering of 1 eV from monolayer to bulk[34]. This is because the parameterization in HSE is performed for bulk systems with isotropic screening and a fixed Hartree–Fock (HF) exchange ratio, which fails to capture the dielectric screening in highly anisotropic ultrathin 2D materials. This ratio needs to be reparameterized depending on the thickness and specific 2D materials used, as based on several recent proposals[34,39,41–45]. This drastic layer-dependent dielectric screening in 2D materials has also been demonstrated by comparing bilayer WSe_2/SnS_2 interfaces with their superlattices, where a type II (bilayer) transition to a type III (superlattice) band alignment was obtained by *GW* calculations, consistent with experimental conductivity measurements[46]. The reason for this is that, within the *GW* approximation, the dielectric screening is accurately included for disparate systems through nonlocal dynamical dielectric matrices, so the layer-dependent quasiparticle energies of 2D materials are accurately described. However, *GW* calculations of supercells with defects are rather computationally intensive, especially for 2D materials, for which numerical convergence is even slower than for their 3D counterparts[47]. Therefore, efficient numerical techniques such as without-explicit-empty-state methods based on density functional perturbation theory can make the computation much more scalable and affordable[48–50], as done in recent work on charged defects in hBN[33,34]. Note that explicit benchmarking of energy levels of defects in 2D materials against experiments has been difficult to perform due to the challenge of identifying exact defects experimentally.

Photophysics modeling of 2D quantum defects

Strong optical transitions and a high quantum yield, where a given defect has a faster radiative recombination rate (with emission of photons) relative to its non-radiative rate (without photon emission), are required for efficient quantum information readout. Accurately predicting these properties for defects in 2D materials presents additional challenges compared with their 3D counterparts because of anisotropic and reduced dielectric screening. In 2D systems, electron–hole pairs generated by absorbed light strongly bind to defect centers because of the large exciton binding energies in 2D systems. Theoretical and computational methodologies for the accurate description of excitonic effects and electron correlation are thus required.

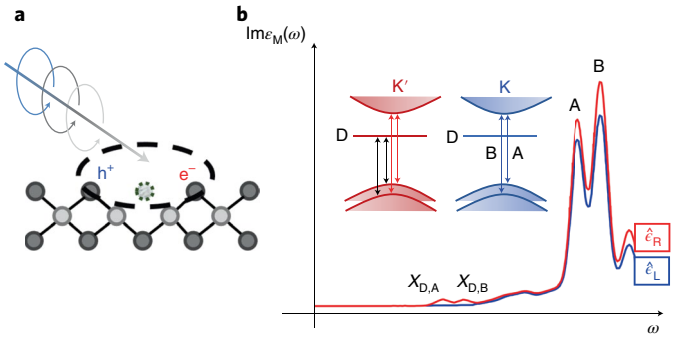

Fig. 4 | Defect-induced optical properties in monolayer $MoSe_2$. **a**, A vacancy defect (missing atom, dashed circle) bound electron (e^-) and hole (h^+) pair (exciton) is generated by circularly polarized light. **b**, Inset: schematic of the band-to-band transition near K and K′ degree for monolayer $MoSe_2$. The transition between the conduction band minimum and the valence band maximum can only be activated by a certain light polarization direction (for K′, red arrows represent left circularly polarized light; for K, blue arrows represent right circularly polarized light). The band-defect transition does not have a preference for the handedness of the light and is represented by black arrows. The red and blue curves in the main plot denote the intensity (in arbitrary units) of the instantaneous emission of left circularly polarized light (red) or right circularly polarized light (blue) from an exciton state excited by right circularly polarized light of the monolayer $MoSe_2$ with the Se vacancy. The presence of the Se vacancy causes the difference in the emission intensity of the left (blue curve) and right (red curve) circularly polarized light[6]. A and B represent the first two transitions between band edges; D represents the defect state in the gap; $X_{D,A}$ represents the transition between the valence band maximum to defect state D; $X_{D,B}$ represents the transition between the second valence band to defect state D. Panel **b** adapted with permission from ref. [6], APS.

Optical excitations for defects in two dimensions. Point defects in TMDs are among the most intriguing candidates as SPEs. There are outstanding questions regarding intrinsic point defects related to the nature of the host materials, where rich excitonic physics exists. Owing to broken inversion symmetry and large spin–orbit couplings[51], monolayer TMDs feature spin–valley locking and selective excitation of states in different valleys by circularly polarized light[52,53]. Meanwhile, the bandgaps of TMDs are rather moderate (1–2 eV) while the exciton binding energy is often large (>500 meV), so optical transitions between bulk states and defect states can hybridize and cause 'valley depolarization'[6]. Figure 4 shows an example of the optical spectra of a Se vacancy in $MoSe_2$ computed by solving the BSE with spin–orbit coupling[6]. The transition between bulk and defect states from a single Se vacancy leads to incomplete circular dichroism for the A and B excitons and a difference of emission intensity between left (blue curve, Fig. 4b) and right (red curve, Fig. 4b) circularly polarized light. In addition, these 2D defects can possess much larger spin–orbit splitting than the bulk states, as obtained in *GW* calculations and experimental scanning tunneling spectroscopy (STS) measurements for a S vacancy in WS_2 (ref. [51]).

From a computational perspective, similar to *GW* calculations, numerical convergence of BSE calculations for the absorption spectra of defects in 2D materials is also extremely challenging. In particular, *k*-point sampling convergence is even slower than for *GW*

calculations. To solve this issue, a non-uniform k-point sampling technique was proposed for ultrathin 2D materials to speed up the k-point convergence and obtain a more accurate description of optical absorption spectra at the long-wavelength limit (photon wavevector $q \to 0$)[54]. The difficulties of convergence with the bands and the dielectric matrix in solving the BSE may be overcome by formulating the BSE without empty states[55–58], which uses density-matrix perturbation theory and the projective dielectric eigenpotential method to avoid explicit empty states and inversion of the dielectric matrix, with a favorable $O(N^4)$ scaling. Use of the Liouville–Lanczos algorithm[58] further speeds up the calculation of absorption spectra over a wide range of frequencies. Recently, this approach was further developed with a direct evaluation of the screened Coulomb interaction in a finite field[59] that eliminates the need to compute dielectric matrices altogether and substantially reduces the cost even further. Furthermore, GW and BSE calculations for open shell systems, such as defects with triplet ground states, carry additional challenges[60]; for example, calculations of the characteristic multiplet structure require a precise knowledge of the frequency dependence of the self-energy, necessary to locate its poles[61], which requires further methodology development for a general solution.

Another theoretical challenge is to estimate the lifetime of optically excited states. The lifetime, which influences the quantum efficiency of SPEs and the readout efficiency of qubits, is determined by the relative ratio of the radiative recombination rate to the non-radiative recombination rate. In the following sections, we discuss the recent developments in calculating radiative and non-radiative lifetimes.

Radiative lifetime. Similar to optical excitations, defect–exciton interactions strongly affect the electron–hole radiative recombination lifetime at defect centers. The radiative lifetime can be calculated using Fermi's golden rule, through which the radiative decay rate (the inverse of the lifetime) from an initial excited state $|S(\mathbf{Q}), 0\rangle$ ($\mathbf{Q}$ is the exciton momentum) to the electronic ground state $|G, 1_{\mathbf{q},\lambda}\rangle$ is given by

$$\gamma(\mathbf{Q}) = \frac{2\pi}{\hbar} \sum_{\mathbf{q},\lambda} \left| \left\langle G, 1_{\mathbf{q},\lambda} \left| H^{\mathrm{int}} \right| S(\mathbf{Q}), 0 \right\rangle \right|^2 \delta(\hbar E_{\mathrm{s}}(\mathbf{Q}) - \hbar c q), \quad (3)$$

where H^{int} is the Hamiltonian describing the interaction between electrons and photons, and E_{s} is the exciton energy at finite exciton momentum. By invoking momentum and energy conservation between a photon and exciton, the dimensionality of the system will yield a different power-law dependence of the radiative rate at the long-wavelength limit of the photon wavevector ($q \to 0$), denoted as γ_0, on the excitation energy. The exciton dipole moment (transition matrix elements), as well as exciton energies E_s, can be obtained by solving the BSE, which includes excitonic effects[62–64]. Excellent agreement between theoretical predictions and experiments for the exciton radiative lifetime has been reported for several pristine 2D semiconductors at finite temperatures[65]. Interestingly, the calculations by Wu et al.[63] show that accurate exciton energy dispersion in momentum space may be important for the finite-temperature exciton lifetime of low-dimensional systems[63]. On the other hand, for defects in 2D systems, the description of electron–hole recombination between two defect levels is rather similar to molecules embedded in a 2D dielectric environment at the dilute limit, although this is different from recombination between defect levels and bulk states. Therefore, the radiative lifetime between two defect levels has an expression similar to zero-dimensional systems with a modification of the dielectric constant from the host materials. The effect of defect–exciton coupling on the radiative lifetime has been discussed previously[66,67] for point defects in hBN, where the exciton binding energy was shown to be substantially stronger for defects (for example, over 2 eV) than for bulk states[66,67]. The importance of the excitonic effect on radiative lifetime may vary substantially among defects: in defects with a reasonably short lifetime (for example, tens of nanoseconds for the N anti-site defect in hBN), the inclusion of excitonic effects (and GW correction) may change the lifetime by less than an order of magnitude, but for defects with a long radiative lifetime (for example, 1 μs for Ti substitution of the divacancy in hBN), the excitonic effect can change the lifetime by several orders of magnitude[66]. The theoretical radiative lifetimes for several proposed SPE candidates in hBN are on the scale of tens of nanoseconds, that is, an order of magnitude longer than known experimental photoluminescence lifetimes[68,69]. It is possible that this overestimation of lifetime may be either due to the lack of exciton–phonon coupling in current calculations, which may be important at room temperature[70], or due to the missing consideration of non-radiative lifetime, which will affect the photoluminescence lifetime and will be discussed next.

Non-radiative lifetime. Non-radiative processes of quantum defects in 2D materials are mostly phonon-assisted transitions. The multi-phonon emission process is often necessary for energy conservation between electronic and phonon energies, especially for deep defect levels in 2D wide-bandgap semiconductors. Under Fermi's golden rule, with electron–phonon coupling, non-radiative phonon-assisted recombination rates can be expressed by[71,72]

$$\gamma = \frac{2\pi}{\hbar} g \sum_m \omega_m \sum_n \left| \Delta H^{\mathrm{e-ph}}_{\mathrm{im;fn}} \right|^2 \delta(E_{\mathrm{im}} - E_{\mathrm{fn}}) \quad (4)$$

where ω_m is the Bose–Einstein occupation of the vibrational state m, and E_{im} and E_{fn} are the energies of the initial and final vibronic states. $\Delta H^{\mathrm{e-ph}}_{\mathrm{im;fn}}$ is the electron–phonon coupling matrix element[73], which has been further simplified using the static coupling approximation[72], where the electronic transition occurs between adiabatic eigenstates for fixed nuclear coordinates. Two main issues remain in the practical implementation. The first issue is the high cost of calculating electron–phonon coupling matrix elements for large supercells containing one point defect, which may be mitigated by a new variational principle algorithm[74]. The second issue is the harmonic approximation for the phonon modes assumed at different defect charge states. Several methods have been proposed to address this issue, including solving the Schrödinger equation using the Fourier grid method along the 1D reaction coordinates[75] or taking into account the local phonon-mode variations for different charge states of a defect with full phonon calculations[76]. In contrast to 3D systems, defects in 2D systems such as hBN experience more dominant defect-to-defect state recombination over defect-to-bulk state recombination[17]. Another unique feature of defects in 2D materials is their high tunability of the non-radiative lifetime as a function of strain[17], as shown in Fig. 5a. The calculated non-radiative lifetime of the N_BV_N defect in hBN (τ_{NR}) decreases an order of magnitude by 1% strain with an expanding strain perpendicular to its C_2 axis[17] due to increased electron–phonon couplings. More importantly, it can lower the quantum yield with the relation $QY = \frac{1/\tau_R}{1/\tau_R + 1/\tau_{NR}}$. The theoretically predicted[17] strain signature of N_BV_N was also validated by subsequent experiments, showing a similar redshift in the zero phonon line and wider photoluminescence spectra[77] (indicating stronger electron–phonon coupling, as depicted at the bottom of Fig. 5a).

Another important non-radiative process for spin qubits takes place through spin–orbit-mediated singlet–triplet intersystem crossing (ISC), as shown by γ_{ISC} in the many-electron-state diagram of a spin defect in Fig. 5b. A rate equation similar to equation (4) can be derived for the ISC rate, γ_{ISC}:

$$\gamma_{\mathrm{ISC}} = 4\pi\hbar\lambda^2 \tilde{X}_{if}(T), \quad (5)$$

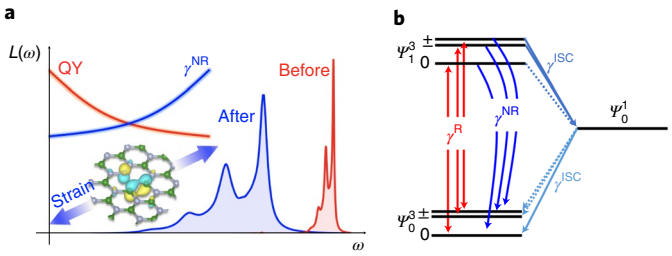

Fig. 5 | Photoluminescence spectra and excited-state decay rates at quantum defects in 2D systems. a, Strain modification of the photoluminescence spectra and non-radiative lifetime (γ^{NR}) of the N_BV_N defect in hBN. The non-radiative rate (blue line) is strongly increased by an applied strain (blue arrow), and the quantum yield (red line) is decreased due to the enhanced non-radiative process. The photoluminescence lineshape ($L(\omega)$) as a function of photon frequency ω L from an SPE in hBN shows a smaller zero phonon line energy (to the left) after applied strain as well as broader spectra ('After', blue curve) with reduced intensity[77], which may be related to the increased electron–phonon coupling (shorter non-radiative lifetime), as theoretically predicted[17]. **b**, The radiative (γ^R) and non-radiative (γ^{NR}) recombination rates, including triplet–singlet ISC rates (γ^{ISC}) for a spin-triplet defect. Ψ_0^3, Ψ_1^3 and Ψ_0^1 represent the triplet ground state, triplet excited state and singlet excited state, respectively.

where $\tilde{X}_{if}(T)$ contains the phonon wavefunction overlap and energy conservation between the electronic and phonon states, T is temperature, i and f represent the initial and final states, respectively, and λ is the spin–orbit coupling constant, which can be computed by time-dependent DFT[78]. Equation (5) implicitly assumes that the spin–orbit coupling constant remains fixed, independent of the coordinates of the atoms, analogous to the Condon approximation on optical excitation[79,80]. $\tilde{X}_{if}$ can be further expressed with phonon wavefunction overlaps, and then computed with the Huang–Rhys approximation[79,81] or (recently) with explicit phonon wavefunctions[66]. The latter method does not require the same phonon frequency for the initial and final defect states, unlike the Huang–Rhys method. Excellent agreement with experimental ISC rates of the NV center has been obtained by both above methods[66,79]. All of the radiative (γ_R) and non-radiative (γ_{NR}, γ_{ISC})$_2$ rates (depicted in Fig. 5b) determine, together, the efficiency of spin state initialization and quantum information readout through photons. Alternately, non-radiative rates can be computed using ab initio non-adiabatic molecular dynamics with the decoherence-corrected surface-hopping algorithm[82,83]. This approach was pioneered by the groups of Prezhdo and Batista[84,85] and has been widely adopted in the quantum chemistry community for photochemistry, for example, for excited electron relaxation. Within non-adiabatic molecular dynamics, the fewest-switches surface-hopping approach within the single-particle description[86,87] is combined with the classical-path approximation, which assumes a classical equilibrium path and that surface hops do not significantly influence the nuclear dynamics. Using such methods, strategies to suppress non-radiative recombination have been discussed in recent works for defects in 2D materials[88,89]. For example, in WSe_2 monolayers, it was found that a W vacancy and Se_W anti-site defects accelerate charge trapping, which means that materials engineering should avoid such defects to properly advance the design of WSe_2 photoactive devices[88]. On the other hand, in monolayer black phosphorus, defect states do not significantly accelerate charge recombination due to the flexibility of the material[89].

The role of exciton–phonon coupling. For defect properties in 2D materials, exciton–phonon coupling may play an important role in determining the excited-state geometry, radiative/non-radiative lifetimes and photoluminescence lineshape (Fig. 2). Several distinct methodologies for exciton–phonon coupling have been developed[81,90–93] and successfully applied for relatively simple bulk systems[81,91–93] or molecules[94]. Computing excited-state forces by solving the BSE has shown promising results for the excited-state geometry of small molecules[94] and, in principle, is applicable to extended systems such as defects in 2D materials (if computationally affordable). Other methods based on many-body perturbation theory that solve the BSE on top of the Fan or Debye–Waller self-energy[81,95] or based on exciton–phonon coupling matrix elements with perturbation theory at a first-order approximation[93] have shown success in capturing accurate finite-temperature absorption spectra and the phonon-assisted photoluminescence lineshape. However, for defect-related excited-state properties, anharmonicity or multi-phonon processes may be important, beyond a first-order approximation. Other important features such as phonon satellites in the strong exciton–phonon coupling regime can be difficult to capture using Fan–Migdal and Debye–Waller self-energies[96]. Methods based on finite-difference exciton–phonon coupling[91] or the stochastic importance sampling Monte Carlo method[92], which can capture electron–phonon coupling to high orders, may be promising for treating defects. In particular, the stochastic importance sampling Monte Carlo method[92] only needs one BSE calculation on a single optimal supercell configuration of atomic positions through stochastic sampling to obtain temperature-dependent optical spectra, which, in the future, would be computationally more affordable than other methods for large supercell defect calculations.

Further challenges in the field

Looking ahead, there are many avenues for future research into 2D quantum defects. For example, an important challenge that needs to be addressed is the accurate description of strongly correlated states. The strong correlation of defect states arises from the interaction of defect orbitals with extended defect resonances and band states, such as the excited singlet state at the NV center in diamond. These strongly correlated states are difficult to treat with methods using a single Slater determinant, such as DFT or *GW*/BSE. Methods such as dynamical mean-field theory, quantum Monte Carlo and configuration interactions have been proposed to address this, but they are computationally expensive for defect supercell calculations. Quantum-embedding theory[97], which combines the above high-level theories for selected degrees of freedom (defined by a chosen active space, related to spin defects) with mean-field theories for the rest of the system[98,99], is a promising pathway for balancing accuracy and computational cost, and has been applied to a few solid-state defects such as the NV center in diamond[100] and a negatively charged B vacancy (V_B^-) in hBN[23].

Another important challenge is the accurate description of excited-state potential energy surfaces and dynamics. Special care is needed for complex potential energy surfaces at excited states, with dynamical Jahn–Teller distortion and spin–orbital-induced ISC. Most available calculations of excited-state geometry have largely been computed with constrained DFT with fixed occupation number, the accuracy of which has yet to be extensively benchmarked against higher levels of theory, such as the density-matrix renormalization group[101] technique or experimental transient spectroscopy. In-depth and comprehensive investigations have been carried out for NV centers in diamond and corroborated with experiments[102], and comparative investigations are in an early stage for 2D defects.

For quantum information applications, the accurate computation of spin relaxation (T_1) and coherence (T_2) times for 2D defects is essential but challenging. T_1 and T_2 are critical parameters for the stable operation of spin qubits, as it is critical for times to be long enough to avoid loss of information. Theoretical predictions of these quantities are thus key to the rational design of spin defects

(as shown in Fig. 2). At low temperature and with a strong magnetic field, spin decoherence is dominated by electron spin–nuclei spin interactions, which induce a fluctuating magnetic field. Recent developments on combining spin Hamiltonians with first-principles inputs and a cluster expansion technique were able to provide an accurate spin Hahn-echo coherence time T_2 that showed excellent agreement with low-temperature experiments for NV centers in diamond[103]. The T_2 for spin defects in 2D materials increases with a reduction in layer thickness, and this enhancement relative to bulk is more prominent at lower nuclear spin concentrations[104]. At elevated temperatures, other effects start to play an important role, such as electron–phonon couplings, which cause spin relaxation and decoherence through spin–orbit interactions. A recent development in relation to spin–phonon relaxation time (T_1) with the density-matrix formalism established the first-principles framework for the spin relaxation time of general solid-state systems[105]. The T_1 due to spin–spin interactions has been computed based on Fermi's golden rule for the NV center in diamond, by combining a spin Hamiltonian with the effective spin–phonon interaction potential[106]. Real-time density-matrix dynamics with various scattering processes will provide a more complete picture of the dominant mechanism under different conditions of temperature, external field and impurity concentrations. For defects in 2D materials in particular, the electron–hole interaction will again be critical in relaxation and decoherence processes and, in the density-matrix formalism, will require a two-particle density matrix and screened nonlocal exchange interactions between an electron and hole. Computationally, this is very challenging, yet it is urgently needed for the reliable predictions of quantum decoherence for spin defects in 2D materials.

Two-dimensional defects can exhibit rich many-body physics and, in recent years, they have stimulated active theoretical developments. First-principles predictions of their electronic, optical and spin properties will provide unbiased and unprecedented insights for designing new quantum defects and for effectively controlling existing ones (such as spin qubits or SPEs), which will be critical for emerging quantum information technologies and spin-optoelectronic applications.

Received: 7 March 2021; Accepted: 15 September 2021;
Published online: 21 October 2021

References

1. Exarhos, A. L., Hopper, D. A., Grote, R. R., Alkauskas, A. & Bassett, L. C. Optical signatures of quantum emitters in suspended hexagonal boron nitride. *ACS Nano* **11**, 3328–3336 (2017).
2. He, Y. et al. Single quantum emitters in monolayer semiconductors. *Nat. Nanotechnol.* **10**, 497–502 (2015).
3. Chakraborty, C., Kinnischtzke, L., Goodfellow, K. M., Beams, R. & Vamivakas, A. N. Voltage-controlled quantum light from an atomically thin semiconductor. *Nat. Nanotechnol.* **10**, 507–511 (2015).
4. Koperski, M. et al. Single photon emitters in exfoliated WSe_2 structures. *Nat. Nanotechnol.* **10**, 503–506 (2015).
5. Aharonovich, I. & Toth, M. Quantum emitters in two dimensions. *Science* **358**, 170–171 (2017).
6. Refaely-Abramson, S., Qiu, D. Y., Louie, S. G. & Neaton, J. B. Defect-induced modification of low-lying excitons and valley selectivity in monolayer transition metal dichalcogenides. *Phys. Rev. Lett.* **121**, 167402 (2018).
7. Sajid, A., Ford, M. J. & Reimers, J. R. Single-photon emitters in hexagonal boron nitride: a review of progress. *Rep. Prog. Phys.* **83**, 044501 (2020).
8. Exarhos, A., Hopper, D., Patel, R., Doherty, M. & Bassett, L. Magnetic-field-dependent quantum emission in hexagonal boron nitride at room temperature. *Nat. Commun.* **10**, 222 (2019).
9. Weber, J. R. et al. Quantum computing with defects. *Proc. Natl Acad. Sci. USA* **107**, 8513–8518 (2010).
10. Ivady, V., Abrikosov, I. A. & Gali, A. First principles calculation of spin-related quantities for point defect qubit research. *npj Comput. Mater.* **4**, 76 (2018).
11. Mackoit-Sinkeviciene, M., Maciaszek, M., Van de Walle, C. G. & Alkauskas, A. Carbon dimer defect as a source of the 4.1-eV luminescence in hexagonal boron nitride. *Appl. Phys. Lett.* **115**, 212101 (2019).
12. Mendelson, N. et al. Identifying carbon as the source of visible single-photon emission from hexagonal boron nitride. *Nat. Mater.* **20**, 321–328 (2021).
13. Sajid, A. & Thygesen, K. S. VNCB defect as source of single photon emission from hexagonal boron nitride. *2D Mater.* **7**, 031007 (2020).
14. Turiansky, M. E., Alkauskas, A., Bassett, L. C. & Van de Walle, C. G. Dangling bonds in hexagonal boron nitride as single-photon emitters. *Phys. Rev. Lett.* **123**, 127401 (2019).
15. Turiansky, M. E. & Van de Walle, C. G. Impact of dangling bonds on properties of h-BN. *2D Mater.* **8**, 024002 (2021).
16. Li, S. et al. Giant shift upon strain on the fluorescence spectrum of VNNB color centers in h-BN. *npj Quantum Inf.* **6**, 85 (2020).
17. Wu, F., Smart, T. J., Xu, J. Q. & Ping, Y. Carrier recombination mechanism at defects in wide band gap two-dimensional materials from first principles. *Phys. Rev. B* **100**, 081407 (2019).
18. Sajid, A., Reimers, J. R., Kobayashi, R. & Ford, M. J. Theoretical spectroscopy of the VNNB defect in hexagonal boron nitride. *Phys. Rev. B* **102**, 144104 (2020).
19. Gupta, S., Yang, J. H. & Yakobson, B. I. Two-level quantum systems in two-dimensional materials for single photon emission. *Nano Lett.* **19**, 408–414 (2019).
20. Klein, J. et al. Engineering the luminescence and generation of individual defect emitters in atomically thin MoS_2. *ACS Photon.* **8**, 669–677 (2021).
21. Zhou, X. C., Zhang, Z. H. & Guo, W. L. Dislocations as single photon sources in two-dimensional semiconductors. *Nano Lett.* **20**, 4136–4143 (2020).
22. Hamdi, H., Thiering, G., Bodrog, Z., Ivady, V. & Gali, A. Stone-Wales defects in hexagonal boron nitride as ultraviolet emitters. *npj Comput. Mater.* **6**, 178 (2020).
23. Ivady, V. et al. Ab initio theory of the negatively charged boron vacancy qubit in hexagonal boron nitride. *npj Comput. Mater.* **6**, 41 (2020).
24. Reimers, J. R. et al. Photoluminescence, photophysics and photochemistry of the VB-defect in hexagonal boron nitride. *Phys. Rev. B* **102**, 144105 (2020).
25. Gottscholl, A. et al. Initialization and read-out of intrinsic spin defects in a van der Waals crystal at room temperature. *Nat. Mater.* **19**, 540–545 (2020).
26. Manson, N. B., Harrison, J. P. & Sellars, M. J. Nitrogen-vacancy center in diamond: model of the electronic structure and associated dynamics. *Phys. Rev. B* **74**, 104303 (2006).
27. Lany, S. & Zunger, A. Assessment of correction methods for the band-gap problem and for finite-size effects in supercell defect calculations: case studies for ZnO and GaAs. *Phys. Rev. B* **78**, 235104 (2008).
28. Wang, D. et al. Determination of formation and ionization energies of charged defects in two-dimensional materials. *Phys. Rev. Lett.* **114**, 196801 (2015).
29. Freysoldt, C. et al. First-principles calculations for point defects in solids. *Rev. Mod. Phys.* **86**, 253–305 (2014).
30. Freysoldt, C., Neugebauer, J. & Van de Walle, C. G. Fully ab initio finite-size corrections for charged-defect supercell calculations. *Phys. Rev. Lett.* **102**, 016402 (2009).
31. Komsa, H. P., Berseneva, N., Krasheninnikov, A. V. & Nieminen, R. M. Charged point defects in the flatland: accurate formation energy calculations in two-dimensional materials. *Phys. Rev. X* **4**, 031044 (2014).
32. Komsa, H. P. & Pasquarello, A. Finite-size supercell correction for charged defects at surfaces and interfaces. *Phys. Rev. Lett.* **110**, 095505 (2013).
33. Wu, F., Galatas, A., Sundararaman, R., Rocca, D. & Ping, Y. First-principles engineering of charged defects for two-dimensional quantum technologies. *Phys. Rev. Mater.* **1**, 071001 (2017).
34. Smart, T. J., Wu, F., Govoni, M. & Ping, Y. Fundamental principles for calculating charged defect ionization energies in ultrathin two-dimensional materials. *Phys. Rev. Mater.* **2**, 124002 (2018).
35. Sundararaman, R. & Ping, Y. First-principles electrostatic potentials for reliable alignment at interfaces and defects. *J. Chem. Phys.* **146**, 104109 (2017).
36. Zhu, G. J., Yang, J. H. & Gong, X. G. Self-consistently determining structures of charged defects and defect ionization energies in low-dimensional semiconductors. *Phys. Rev. B* **102**, 035202 (2020).
37. Xia, S. et al. Evaluation of charged defect energy in two-dimensional semiconductors for nanoelectronics: the WLZ extrapolation method. *Ann. Phys.* **532**, 1900318 (2020).
38. da Silva, M. et al. Self-consistent potential correction for charged periodic systems. *Phys. Rev. Lett.* **126**, 076401 (2021).
39. Elliott, J. D., Colonna, N., Marsili, M., Marzari, N. & Umari, P. Koopmans meets Bethe-Salpeter: excitonic optical spectra without GW. *J. Chem. Theory Comput.* **15**, 3710–3720 (2019).
40. Heyd, J., Scuseria, G. E. & Ernzerhof, M. Hybrid functionals based on a screened Coulomb potential. *J. Chem. Phys.* **118**, 8207–8215 (2003).
41. Miceli, G., Chen, W., Reshetnyak, I. & Pasquarello, A. Nonempirical hybrid functionals for band gaps and polaronic distortions in solids. *Phys. Rev. B* **97**, 121112 (2018).

42. Nguyen, N. L., Colonna, N., Ferretti, A. & Marzari, N. Koopmans-compliant spectral functionals for extended systems. *Phys. Rev. X* **8**, 021051 (2018).
43. Brawand, N. P., Govoni, M., Voros, M. & Galli, G. Performance and self-consistency of the generalized dielectric dependent hybrid functional. *J. Chem. Theory Comput.* **13**, 3318–3325 (2017).
44. Chen, W., Miceli, G., Rignanese, G. M. & Pasquarello, A. Nonempirical dielectric-dependent hybrid functional with range separation for semiconductors and insulators. *Phys. Rev. Mater.* **2**, 073803 (2018).
45. Zheng, H. H., Govoni, M. & Galli, G. Dielectric-dependent hybrid functionals for heterogeneous materials. *Phys. Rev. Mater.* **3**, 073803 (2019).
46. Zhao, B. et al. High-order superlattices by rolling up van der Waals heterostructures. *Nature* **591**, 385–390 (2021).
47. Qiu, D. Y., da Jornada, F. H. & Louie, S. G. Optical spectrum of MoS_2: many-body effects and diversity of exciton states. *Phys. Rev. Lett.* **111**, 216805 (2013).
48. Govoni, M. & Galli, G. Large scale GW calculations. *J. Chem. Theory Comput.* **11**, 2680–2696 (2015).
49. Nguyen, H., Pham, T., Rocca, D. & Galli, G. Improving accuracy and efficiency of calculations of photoemission spectra within the many-body perturbation theory. *Phys. Rev. B* **85**, 081101(R) (2012).
50. Pham, T., Nguyen, H., Rocca, D. & Galli, G. GW calculations using the spectral decomposition of the dielectric matrix: verification, validation and comparison of methods. *Phys. Rev. B* **87**, 155148 (2013).
51. Schuler, B. et al. Large spin–orbit splitting of deep in-gap defect states of engineered sulfur vacancies in monolayer WS_2. *Phys. Rev. Lett.* **123**, 076801 (2019).
52. Liu, Y. P. et al. Valleytronics in transition metal dichalcogenides materials. *Nano Res.* **12**, 2695–2711 (2019).
53. Srivastava, A. et al. Valley Zeeman effect in elementary optical excitations of monolayer WSe_2. *Nat. Phys.* **11**, 141–147 (2015).
54. da Jornada, F. H., Qiu, D. Y. & Louie, S. G. Nonuniform sampling schemes of the Brillouin zone for many-electron perturbation-theory calculations in reduced dimensionality. *Phys. Rev. B* **95**, 035109 (2017).
55. Ping, Y., Rocca, D., Lu, D. & Galli, G. Ab initio calculations of absorption spectra of semiconducting nanowires within many-body perturbation theory. *Phys. Rev. B* **85**, 035316 (2012).
56. Ping, Y., Rocca, D. & Galli, G. Electronic excitations in light absorbers for photoelectrochemical energy conversion: first principles calculations based on many body perturbation theory. *Chem. Soc. Rev.* **42**, 2437–2469 (2013).
57. Rocca, D., Ping, Y., Gebauer, R. & Galli, G. Solution of the Bethe-Salpeter equation without empty electronic states: application to the absorption spectra of bulk systems. *Phys. Rev. B* **85**, 045116 (2012).
58. Rocca, D., Lu, D. & Galli, G. Ab initio calculations of optical absorption spectra: solution of the Bethe-Salpeter equation within density matrix perturbation theory. *J. Chem. Phys.* **133**, 164109 (2010).
59. Nguyen, N., Ma, H., Govoni, M., Gygi, F. & Galli, G. Finite-field approach to solving the Bethe-Salpeter equation. *Phys. Rev. Lett.* **122**, 237402 (2019).
60. Stoughton, S. et al. Adsorption-controlled growth of $BiVO_4$ by molecular-beam epitaxy. *APL Mater.* **1**, 042112 (2013).
61. Lischner, J., Deslippe, J., Jain, M. & Louie, S. G. First-principles calculations of quasiparticle excitations of open-shell condensed matter systems. *Phys. Rev. Lett.* **109**, 036406 (2012).
62. Spataru, C. D., Ismail-Beigi, S., Capaz, R. B. & Louie, S. G. Theory and ab initio calculation of radiative lifetime of excitons in semiconducting carbon nanotubes. *Phys. Rev. Lett.* **95**, 247402 (2005).
63. Wu, F., Rocca, D. & Ping, Y. Dimensionality and anisotropicity dependence of radiative recombination in nanostructured phosphorene. *J. Mater. Chem. C* **7**, 12891–12897 (2019).
64. Chen, H. Y., Jhalani, V. A., Palummo, M. & Bernardi, M. Ab initio calculations of exciton radiative lifetimes in bulk crystals, nanostructures and molecules. *Phys. Rev. B* **100**, 075135 (2019).
65. Palummo, M., Bernardi, M. & Grossman, J. C. Exciton radiative lifetimes in two-dimensional transition metal dichalcogenides. *Nano Lett.* **15**, 2794–2800 (2015).
66. Smart, T., Li, K., Xu, J. & Ping, Y. Intersystem crossing and exciton-defect coupling of spin defects in hexagonal boron nitride. *npj Comput. Mater.* **7**, 59 (2021).
67. Gao, S., Chen, H.-Y. & Bernardi, M. Radiative properties of quantum emitters in boron nitride from excited state calculations and Bayesian analysis. *npj Comput. Mater.* **7**, 85 (2021).
68. Tran, T. T. et al. Robust multicolor single photon emission from point defects in hexagonal boron nitride. *ACS Nano* **10**, 7331–7338 (2016).
69. Schell, A. W., Takashima, H., Tran, T. T., Aharonovich, I. & Takeuchi, S. Coupling quantum emitters in 2D materials with tapered fibers. *ACS Photon.* **4**, 761–767 (2017).
70. Antonius, G. & Louie, S. G. Theory of the exciton-phonon coupling. Preprint at https://arxiv.org/abs/1705.04245 (2017).
71. Alkauskas, A., Yan, Q. M. & Van de Walle, C. G. First-principles theory of nonradiative carrier capture via multiphonon emission. *Phys. Rev. B* **90**, 075202 (2014).
72. Shi, L., Xu, K. & Wang, L. W. Comparative study of ab initio nonradiative recombination rate calculations under different formalisms. *Phys. Rev. B* **91**, 205315 (2015).
73. Giustino, F. Electron-phonon interactions from first principles. *Rev. Mod. Phys.* **89**, 015003 (2017).
74. Shi, L. & Wang, L. Ab initio calculations of deep-level carrier nonradiative recombination rates in bulk semiconductors. *Phys. Rev. Lett.* **109**, 245501 (2012).
75. Zhang, X., Shen, J., Turiansky, M. & Van de Walle, C. Minimizing hydrogen vacancies to enable highly efficient hybrid perovskites. *Nat. Mater.* **20**, 971–976 (2021).
76. Xiao, Y. et al. Anharmonic multi-phonon nonradiative transition: an ab initio calculation approach. *Sci. China Phys. Mech. Astron.* **63**, 277312 (2020).
77. Mendelson, N., Doherty, M., Toth, M., Aharonovich, I. & Tran, T. T. Strain-induced modification of the optical characteristics of quantum emitters in hexagonal boron nitride. *Adv. Mater.* **32**, 1908316 (2020).
78. de Souza, B., Farias, G., Neese, F. & Izsak, R. Predicting phosphorescence rates of light organic molecules using time-dependent density functional theory and the path integral approach to dynamics. *J. Chem. Theory Comput.* **15**, 1896–1904 (2019).
79. Thiering, G. & Gali, A. Ab initio calculation of spin-orbit coupling for an NV center in diamond exhibiting dynamic Jahn-Teller effect. *Phys. Rev. B* **96**, 081115(R) (2017).
80. Alkauskas, A., Buckley, B., Awschalom, D. & Van de Walle, C. First-principles theory of the luminescence lineshape for the triplet transition in diamond NV centres. *N. J. Phys.* **16**, 073026 (2014).
81. Marini, A. Ab initio finite-temperature excitons. *Phys. Rev. Lett.* **101**, 106405 (2008).
82. Wong, J. C., Li, L. S. & Kauai, Y. Size dependence and role of decoherence in hot electron relaxation within fluorinated silicon quantum dots: a first-principles study. *J. Phys. Chem. C* **122**, 29526–29536 (2018).
83. Stier, W. & Prezhdo, O. Nonadiabatic molecular dynamics simulation of light-induced, electron transfer from an anchored molecular electron donor to a semiconductor acceptor. *J. Phys. Chem. B* **106**, 8047–8054 (2002).
84. Rego, L. & Batista, V. Quantum dynamics simulations of interfacial electron transfer in sensitized TiO_2 semiconductors. *J. Am. Chem. Soc.* **125**, 7989–7997 (2003).
85. Parandekar, P. & Tully, J. Mixed quantum-classical equilibrium. *J. Chem. Phys.* **122**, 094102 (2005).
86. Tully, J. Molecular-dynamics with electronic transitions. *J. Chem. Phys.* **93**, 1061–1071 (1990).
87. Li, L. S. & Carter, E. A. Defect-mediated charge-carrier trapping and nonradiative recombination in WSe_2 monolayers. *J. Am. Chem. Soc.* **141**, 10451–10461 (2019).
88. Zhang, L. L. et al. Suppression of electron-hole recombination by intrinsic defects in 2D monoelemental material. *J. Phys. Chem. Lett.* **10**, 6151–6158 (2019).
89. Ismail-Beigi, S. & Louie, S. Excited-state forces within a first-principles Green's function formalism. *Phys. Rev. Lett.* **90**, 076401 (2003).
90. Cannuccia, E., Monserrat, B. & Attaccalite, C. Theory of phonon-assisted luminescence in solids: application to hexagonal boron nitride. *Phys. Rev. B* **99**, 081109(R) (2019).
91. Zacharias, M., Patrick, C. & Giustino, F. Stochastic approach to phonon-assisted optical absorption. *Phys. Rev. Lett.* **115**, 177401 (2015).
92. Chen, H.-Y., Sangalli, D. & Bernadi, M. Exciton-phonon interaction and relaxation times from first principles. *Phys. Rev. Lett.* **125**, 107401 (2020).
93. Caylak, O. & Baumeier, B. Excited-state geometry optimization of small molecules with many-body Green's functions theory. *J. Chem. Theory Comput.* **17**, 879–888 (2021).
94. Molina-Sanchez, A., Palummo, M., Marini, A. & Wirtz, L. Temperature-dependent excitonic effects in the optical properties of single-layer MoS_2. *Phys. Rev. B* **93**, 155435 (2016).
95. Nery, J. et al. Quasiparticles and phonon satellites in spectral functions of semiconductors and insulators: cumulants applied to the full first-principles theory and the Frohlich polaron. *Phys. Rev. B* **97**, 115145 (2018).
96. Ma, H., Sheng, N., Govoni, M. & Galli, G. Quantum embedding theory for strongly correlated states in materials. *J. Chem. Theory Comput.* **17**, 2116–2125 (2021).
97. Barcza, G. et al. DMRG on top of plane-wave Kohn-Sham orbitals: a case study of defected boron nitride. *J. Chem. Theory Comput.* **17**, 1143–1154 (2021).
98. Ma, H., Govoni, M. & Galli, G. Quantum simulations of materials on near-term quantum computers. *npj Comput. Mater.* **6**, 85 (2020).

99. Ma, H., Sheng, N., Govoni, M. & Galli, G. First-principles studies of strongly correlated states in defect spin qubits in diamond. *Phys. Chem. Chem. Phys.* **22**, 25522–25527 (2020).
100. Hu, W. & Chan, G. Excited-state geometry optimization with the density matrix renormalization group, as applied to polyenes. *J. Chem. Theory Comput.* **11**, 3000–3009 (2015).
101. Gali, A. Ab initio theory of the nitrogen-vacancy center in diamond. *Nanophotonics* **8**, 1907–1943 (2019).
102. Seo, H. et al. Quantum decoherence dynamics of divacancy spins in silicon carbide. *Nat. Commun.* **7**, 12935 (2016).
103. Ye, M., Seo, H. & Galli, G. Spin coherence in two-dimensional materials. *npj Comput. Mater.* **5**, 44 (2019).
104. Xu, J. Q. et al. Spin–phonon relaxation from a universal ab initio density-matrix approach. *Nat. Commun.* **11**, 2780 (2020).
105. Gugler, J. et al. Ab initio calculation of the spin lattice relaxation time T_1 for nitrogen-vacancy centers in diamond. *Phys. Rev. B* **98**, 214442 (2018).
106. Jaeger, H. M., Fischer, S. & Prezhdo, O. V. Decoherence-induced surface hopping. *J. Chem. Phys.* **137**, 22A545 (2012).

Acknowledgements

This material is based on work supported by the Air Force Office of Scientific Research under AFOSR award no. FA9550-YR-1-XYZQ and National Science Foundation under grant no. DMR-1760260. T.J.S. acknowledges support from the LLNL Graduate Research Scholar Program and funding support from LLNL LDRD 20-SI-004.

Author contributions

Y.P. was in charge of the overall direction, planning and writing. T.J.S. contributed to the figures and partially to writing the manuscript.

Competing interests

The authors declare no competing interests.

Additional information

Correspondence should be addressed to Yuan Ping.

Peer review information *Nature Computational Science* thanks the anonymous reviewers for their contribution to the peer review of this work. Handling editor: Jie Pan, in collaboration with the *Nature Computational Science* team.

Reprints and permissions information is available at www.nature.com/reprints.

Publisher's note Springer Nature remains neutral with regard to jurisdictional claims in published maps and institutional affiliations.